The Astronomical Journal, 146:39 (12pp), 2013 August doi:10.1088/0004-6256/146/2/39

TWO BARIUM STARS IN THE OPEN CLUSTER NGC 5822*

O. J. Katime Santrich, C. B. Pereira, and D. B. de Castro
Observatório Nacional/MCT, Rua Gen. José Cristino, 77, 20921-400 Rio de Janeiro, Brazil; osantrich@on.br, claudio@on.br, denise@on.br
Received 2013 January 16; accepted 2013 May 27; published 2013 July 15

ABSTRACT

Open clusters are very useful examples to explain the constraint of the nucleosynthesis process with the luminosities of stars because the distances of the clusters are better known than those of field stars. We carried out a detailed spectroscopic analysis to derive the chemical composition of two red giants in the young open cluster NGC 5822, NGC 5822-2, and NGC 5822-201. We obtained abundances of C, N, O, Na, Mg, Al, Ca, Si, Ti, Ni, Cr, Y, Zr, La, Ce, and Nd. The atmospheric parameters of the studied stars and their chemical abundances were determined using high-resolution optical spectroscopy. We employed the local thermodynamic equilibrium model atmospheres of Kurucz and the spectral analysis code MOOG. The abundances of the light elements were derived using the spectral synthesis technique. We found that NGC 5822-2 and -201 have, respectively, a mean overabundance of the elements created by the *s*-process, "*s*," with the notation [*s*/Fe] of 0.77 ± 0.12 and 0.83 ± 0.05. These values are higher than those for field giants of similar metallicity. We also found that NGC 5822-2 and -201 have, respectively, luminosities of 140 $L_\odot$ and 76 $L_\odot$, which are much lower than the luminosity of an asymptotic giant branch star. We conclude that NGC 5822-2 and NGC 5822-201 are two new barium stars first identified in the open cluster NGC 5822. The mass transfer hypothesis is the best scenario to explain the observed overabundances.

Key words: open clusters and associations: individual (NGC 5822) – stars: abundances – stars: fundamental parameters – stars: individual (CPD −53°6222, CPD −53°6224)

1. INTRODUCTION

In addition to field stars, H II regions, cepheid variables, and OB stars, open clusters are very useful in probing the chemical evolution of the galaxy. Besides, since we also know their distances, the luminosities of the stars in the cluster are better constrained than the field stars. This is an important stellar parameter because it is often used to constrain stellar evolution models as well as nucleosynthesis processes and dredge-up episodes (Boothroyd & Sackmann 1988; Lattanzio & Wood 2004). Therefore, any chemical enrichment or depletion observed in the spectra of cluster giants may be compared with the predictions of evolutionary models. One important chemical enrichment that is frequently observed in the atmospheres of evolved stars is the overabundance of elements created by slow neutron capture reactions. This process was called *s*-process by Burbidge et al. (1957). Elements heavier than the iron peak ($Z > 30$), such as barium and strontium, are synthesized in this way, provided that the rate of neutron capture is slow compared to the beta-decay timescale of the radioactive nuclei involved in the chain. The main site for this process is inside a star during its evolution through the asymptotic giant branch (AGB) phase, when the star develops helium-burning thermal pulses (TP-AGB phase). A by-product of the thermal pulse is the production of both carbon and neutron-rich isotopes of heavy elements. Theoretical calculations show that in order for the first thermal pulse to develop, a star should present a luminosity of $\simeq$1400 $L_\odot$ (Vassiliadis & Wood 1993). During the TP-AGB phase, material from the He intershell, enriched by carbon and the *s*-process elements, is brought to the star's surface due to the deep convection zone of the AGB star ("third dredge-up"). Therefore, the study of *s*-process elements in the atmospheres of these stars is very useful for setting constraints on the models of neutron capture nucleosynthesis during the AGB. Unfortunately, the atmosphere of the AGB stars is crowded due to a strong molecular opacity that makes the study of the chemical abundances using atomic lines very difficult.

Barium stars are another example of objects that also display element enrichment by the *s*-process. However, barium stars are not luminous enough, and their effective temperatures are too high to be considered AGB stars that underwent a third dredge-up. Therefore, their overabundances of carbon and *s*-process elements are explained by mass transfer in a binary system from a former AGB star (now a white dwarf in the system). Because they are too warm relative to the AGB stars, and have spectral types G and K, barium stars are free from the strong molecular opacity from ZrO, CN, and C_2 absorption features. This makes barium stars ideal to better probe the enrichment of *s*-process nucleosynthesis in the atmospheres of these stars. Several works have already been published about the chemical composition of field barium stars, such as Allen & Barbuy (2006), Smiljanic et al. (2009), and Pereira et al. (2011) to name a few. Since the work of McClure et al. (1974) for the old open cluster NGC 2420 and the subsequent confirmation using high-resolution spectroscopy by Smith & Suntzeff (1987), there was no detection of barium stars in an open cluster. In this work, we report the discovery of two barium stars in the open cluster NGC 5822, NGC 5822-2, and NGC 5822-201. We will show that NGC 5822-2 and NGC 5822-201 have overabundances of *s*-process elements greater than those of the field giant stars of similar metallicity. We will also show that the observed overabundance is similar to the barium stars reported in the literature as well as to the star HD 65314, a barium star used as an *s*-process-enriched template star.

The open cluster NGC 5822 was selected to be observed with high-resolution spectroscopy because we have started a project to obtain the atmospheric parameters and chemical abundances of a sample of red giant stars in several open clusters. This project benefited from the radial-velocity survey done by Mermilliod et al. (2008), where several red giant stars were

* Based on observations made with the 2.2 m telescope at the European Southern Observatory (La Silla, Chile).

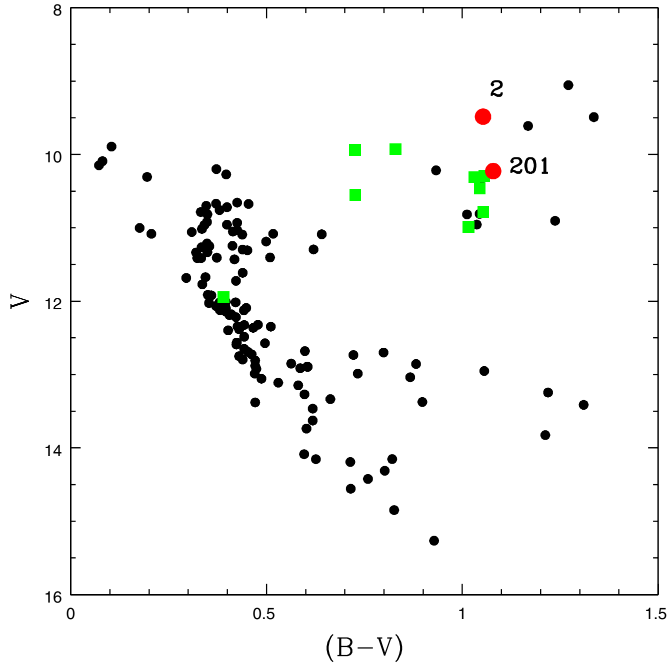

Figure 1. Color–magnitude diagram of the red giants in NGC 5822. Green squares represent the binary stars. The barium stars (red circles) NGC 5822-2 and -201 are also shown. The *UBV* photometry was obtained from Twarog et al. (1993).

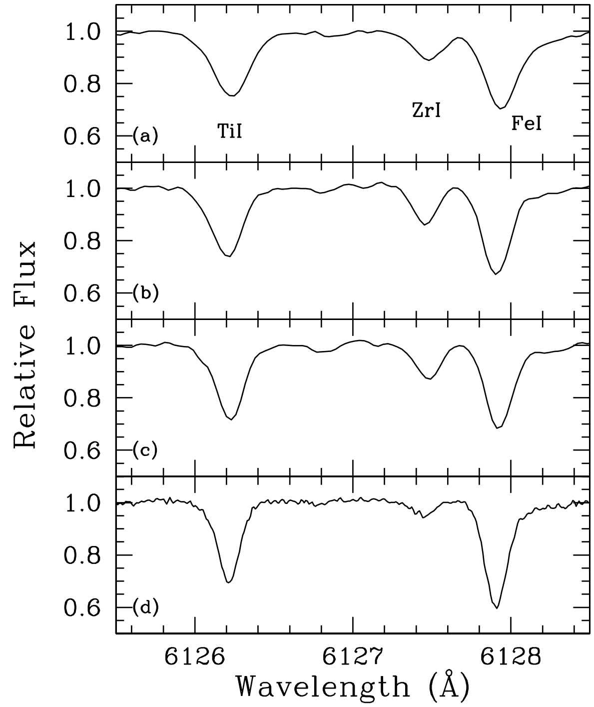

Figure 2. Normalized spectra of the open cluster giants NGC 5822-2 (a) and NGC 5822-201 (b), the barium star HD 65314 (c), and the giant star HD 2114 (d) in the region of the absorption line of Zr I 6127.46 Å.

identified as members of the star clusters surveyed by these authors. For the open cluster NGC 5822, we have observed 15 giant stars, all of which, according to Mermilliod et al. (2008), are members of this cluster, including these two barium giants. Some giant stars of NGC 5822 have already been investigated by several authors through high-resolution spectroscopy—Luck (1994), Santos et al. (2009), Smiljanic et al. (2009), and Pace et al. (2010)—but there has not yet been a study dedicated to analyzing a large sample of giant stars in this cluster.

The confirmation of barium stars in open clusters is important in order to check whether the heavy-element enrichment is due to an *intrinsic* nuclear process or due to an *extrinsic* process, i.e., the mass transfer hypothesis, since the luminosities of the stars in clusters are better constrained by their known distances. NGC 5822-2 and -201 have already been recognized as spectroscopic binaries (Mermilliod et al. 1989; Mermilliod & Mayor 1990); therefore, the detection of barium stars may raise other constraints, such as, for example, the theoretical birthrate of these kind of stars in open clusters compared to field stars as well as for the mixing and dredge-up process and nucleosynthesis on AGB stars. Since they host white dwarfs, barium stars are binary stars whose companions are white dwarfs and (Böhm-Vitense et al. 2000; Gray et al. 2011) can be another important source, other than imaging, for counting and identification of white dwarfs in open clusters (Dobbie et al. 2012). This is important to constrain the ages of the open clusters and can be compared with cluster turnoff ages (von Hippel et al. 1995).

2. OBSERVATIONS

The high-resolution spectra for these two stars were obtained at the 2.2 m ESO telescope of La Silla, Chile using the echelle spectrograph Fiberfed Extended Range Optical Spectrograph (FEROS; Kaufer et al. 1999). The FEROS spectral resolving power is $R = 48{,}000$, corresponding to 2.2 pixels of 15 μm, and has a complete wavelength coverage without gaps from 3800 Å to 9200 Å. The stars were selected from the radial velocity survey of Mermilliod et al. (2008). The nominal signal to noise ratio (S/N) was evaluated by measuring the rms flux fluctuation in selected continuum windows, and in both stars the typical values are around 100. The spectra were reduced with the MIDAS pipeline reduction package consisting of the following standard steps: CCD bias correction, flat fielding, spectrum extraction, wavelength calibration, correction of barycentric velocity, and spectrum rectification. Table 1 gives the log of the observations and other information of the observed stars. In Figure 1, we show the color–magnitude diagram of NGC 5822 using the *UBV* photometry of Twarog et al. (1993) for the red giants in NGC 5822, including the barium giants NGC 5822-2 and -201. The green points represent the binary stars marked by Mermilliod & Mayor (1990). The frequency of known binary stars in open clusters is important to constrain, through *N*-body simulations, the dynamical evolution of the clusters and for comparison with the predicted frequency of blue stragglers (Hurley et al. 2005).

Figures 2, 3, and 4 show the spectra of NGC 5822-2 and -201 for some selected regions where the transitions due to

Table 1
Log of the Observations and Other Relevant Information for the Target Stars

ID	CPD	V	$B-V$	RV[a] (km s^{-1})	RV[b] (km s^{-1})	Date Obs.	Exp. (s)
2	−53°6222	9.55	1.06	−29.20	−25.07 ± 0.50	2009 Mar 7	900
201	−53°6224	10.24	1.07	−27.90	−27.80 ± 0.23	2009 Mar 8	1200

Notes. ID, CPD number, *V*, *B−V*, and radial velocities were taken from Mermilliod et al. (2008) (Columns 1–5). Our values for the radial velocities are given in Column 6. The last two columns provide the dates of observation and exposure times.
[a] Mermilliod et al. (2008).
[b] This work.

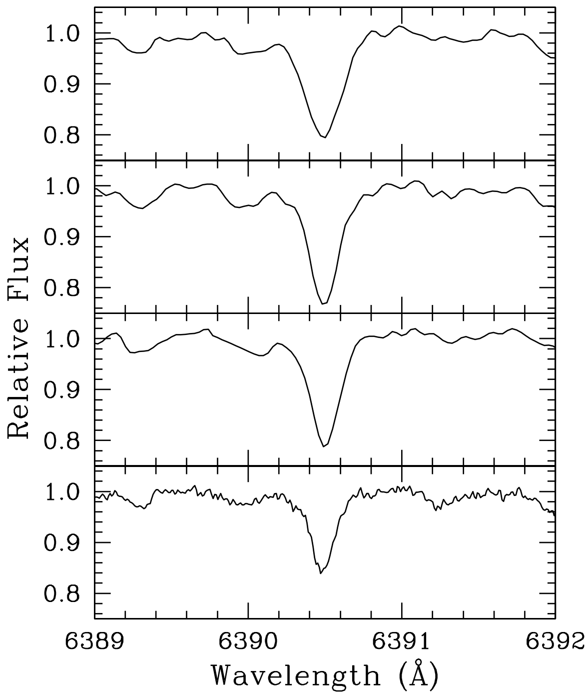

Figure 3. Same as in Figure 2, but for the region of the absorption line of La II 6390.48 Å.

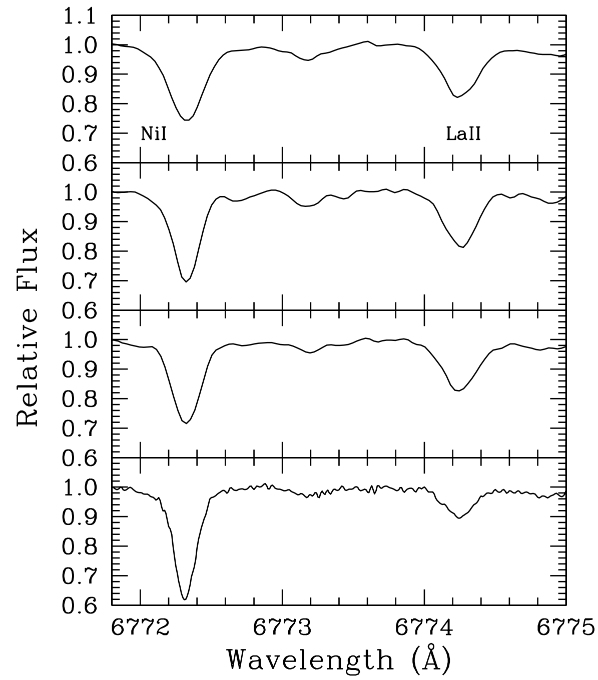

Figure 4. Same as in Figure 2, but for the region of the absorption line of La II 6774.33 Å.

the elements synthesized by the *s*-process are observed. For comparison, these figures also show the spectrum of a barium star, HD 65314, and the spectrum of a non-*s*-process-enriched giant star HD 2114. As we shall see, HD 65314 and HD 2114 have atmospheric parameters similar to those of the two cluster giants. So, the line strengths of these elements are related to the overabundances of these elements in the atmosphere of HD 65314, and, in the case of HD 2114, as a result of normal solar abundance.

3. ANALYSIS AND RESULTS

3.1. Line Selection, Measurement, and Oscillator Strengths

The stellar spectra of the stars analyzed in this work show many atomic absorption lines of Fe I and Fe II as well as transitions due to Na I, Mg I, Al I, Si I, Ca I, Ti I, Cr I, Ni I, Y II, Zr I, La II, Ce II, and Nd II. We have chosen a set of lines sufficiently unblended to yield reliable abundances. Equivalent widths were measured using the task *splot* from IRAF. The selected lines are listed in Table 2 for the case of Fe I and Fe II lines and in Table 3 for the other elements. Tables 2 and 3 also provide the lower excitation potential, χ (eV), of the transitions and the gf values. The gf values for the Fe I and Fe II lines were taken from Lambert et al. (1996) and Castro et al. (1997), and for the other elements the sources of the gf values are given in Table 3.

3.2. Atmospheric Parameters

To obtain the chemical abundances, it is necessary first to calculate the stellar parameters: effective temperature $T_{\rm eff}$, surface gravity log g, metallicity [Fe/H] ($[{\rm X/H}] = \log(N_{\rm X}/N_{\rm H})_\star - \log(N_{\rm X}/N_{\rm H})_\odot$), and microturbulent velocity ξ. The atmospheric parameters were determined using the local thermodynamic equilibrium (LTE) model atmospheres of Kurucz (1993) and the spectral analysis code *MOOG* (Sneden 1973).

The effective temperature was derived by requiring that the abundances calculated for the Fe I lines do not show any dependence upon excitation potential. Thus, the solution thus found is unique, depending only on a set of Fe I and Fe II lines and the employed atmospheric model, and yields as a by-product the metallicity of the star ([Fe/H]). The gravity was determined by forcing the Fe I and Fe II lines to yield the same iron abundance at the selected effective temperature. The microturbulent velocity was determined by forcing the abundance determined from individual Fe I lines to show no dependence on the equivalent width. Results for the stellar parameters are shown in Table 4.

Previous determinations of the atmospheric parameters of NGC 5822-2 and -201 were done, respectively, by Luck (1994) and Smiljanic et al. (2009). The solutions are also shown in Table 4. The observations of Luck (1994) were done with medium resolution ($R = 18{,}000$) while Smiljanic et al. (2009) observed with the FEROS spectrograph. As can be observed in Table 4, our stellar parameters are in good agreement with previous determinations, except for the microturbulence velocity.

As was mentioned earlier, we have compared the spectra of NGC 5822-2 and -201 with the spectrum of barium star HD 65314 and normal giant HD 2114. HD 65314 was also selected as an *s*-process-enriched comparison star after analyzing our results for the stellar parameters and abundances obtained from the large high-resolution spectroscopic survey of the barium stars selected from the samples of MacConnell et al. (1972) and Bidelman (1981) as well as some stars from Gomez et al. (1997). This survey aims to obtain the atmospheric parameters, abundances, and the kinematical properties of these chemically peculiar stars and compare them with the non-*s*-process-enriched giant stars. Of the 230 surveyed stars, we have already discovered a new CH subgiant, BD−03°3668 (Pereira & Drake 2011) as well as a sample of metal-rich barium stars (Pereira et al. 2011). As will be seen in Section 4.2.3, HD 65314 displays a mean *s*-process abundance ([*s*/Fe]) similar to that of

Table 2
Observed Fe I and Fe II Lines

Element	λ (Å)	χ (eV)	log *gf*	EQW_2 (mÅ)	EQW_{201} (mÅ)	EQW_{65314} (mÅ)
Fe I	5159.06	4.28	−0.650	90	100	...
	5162.27	4.18	+0.079	130	...	...
	5198.71	2.22	−2.140	...	133	135
	5242.49	3.63	−0.970	114	109	110
	5250.21	0.12	−4.920	125	113	122
	5253.03	2.28	−3.790	52	44	...
	5288.52	3.69	−1.510	92	81	81
	5307.36	1.61	−2.970	...	132	131
	5315.05	4.37	−1.400	65	49	...
	5321.11	4.43	−1.190	67	64	61
	5322.04	2.28	−2.840	106	92	90
	5364.87	4.45	+0.230	...	134	128
	5367.47	4.42	+0.439	...	...	135
	5373.70	4.47	−0.710	85	80	77
	5389.47	4.42	−0.250	107	...	99
	5410.91	4.47	+0.400	...	133	...
	5417.03	4.42	−1.530	57	...	49
	5441.33	4.31	−1.580	59	59	53
	5445.04	4.39	+0.040	...	128	120
	5522.44	4.21	−1.400	68	63	58
	5532.74	3.57	−2.000	79	68	...
	5560.21	4.43	−1.040	75	71	65
	5576.09	3.43	−0.850	...	...	125
	5624.02	4.39	−1.330	...	...	69
	5633.94	4.99	−0.120	85	...	81
	5635.82	4.26	−1.740	46	44	43
	5638.26	4.22	−0.720	98	94	97
	5686.53	4.55	−0.450	...	93	...
	5691.50	4.30	−1.370	72	70	63
	5705.46	4.30	−1.360	...	57	58
	5717.83	4.28	−0.979	...	86	85
	5731.76	4.26	−1.150	77	78	78
	5806.73	4.61	−0.900	73	72	68
	5814.81	4.28	−1.820	38	35	38
	5852.22	4.55	−1.180	65	54	58
	5883.81	3.96	−1.210	89	81	91
	5916.24	2.45	−2.990	...	91	89
	5934.65	3.93	−1.020	106	100	98
	6024.06	4.55	−0.060	127	114	116
	6027.05	4.08	−1.090	93	83	79
	6056.01	4.73	−0.400	...	82	83
	6079.00	4.65	−0.970	65	61	62
	6082.71	2.22	−3.580	72	66	72
	6093.64	4.61	−1.350	44	44	42
	6096.66	3.98	−1.780	53	53	53
	6120.24	0.91	−5.950	26	...	29
	6151.62	2.18	−3.290	92	84	84
	6165.36	4.14	−1.470	68	60	62
	6173.34	2.22	−2.880	116	108	101
	6187.99	3.94	−1.570	73	73	67
	6200.32	2.60	−2.440	111	103	106
	6213.43	2.22	−2.480	131	122	115
	6265.13	2.18	−2.550	...	132	129
	6311.50	2.83	−3.230	...	49	55
	6322.69	2.59	−2.430	118	109	107
	6380.74	4.19	−1.320	...	...	83
	6392.53	2.28	−4.030	41	36	46
	6411.65	3.65	−0.660	...	...	137
	6419.95	4.73	−0.090	104	103	106
	6436.40	4.19	−2.460	...	25	...
	6551.67	0.99	−5.790	27	27	...
	6574.22	0.99	−5.020	83	70	73
	6593.87	2.44	−2.420	...	...	120
	6597.56	4.79	−0.920	58	58	55
	6608.02	2.28	−4.030	45	46	45
	6609.11	2.56	−2.690	112	...	104
	6646.93	2.61	−3.990	26	31	...
	6699.14	4.59	−2.190	...	...	20
	6703.56	2.76	−3.160	78	72	70
	6704.48	4.22	−2.660	...	...	15
	6713.74	4.79	−1.600	30	29	40
	6739.52	1.56	−4.950	39	29	41
	6745.96	4.07	−2.770	...	...	18
	6750.15	2.42	−2.620	122	113	115
	6752.71	4.64	−1.200	...	63	65
	6783.70	2.59	−3.980	...	...	45
	6793.25	4.07	−2.470	22	20	25
	6806.84	2.73	−3.210	74	68	70
	6810.26	4.61	−1.200	70	75	67
	6820.37	4.64	−1.170	65	62	59
	6841.33	4.61	−0.600	...	84	...
	6858.15	4.61	−0.930	79	73	71
	7132.99	4.08	−1.610	...	...	64
Fe II	4993.35	2.81	−3.670	72	64	56
	4993.35	2.81	−3.670	...	...	56
	5132.65	2.81	−4.000	59	59	48
	5234.62	3.22	−2.240	115	112	103
	5284.10	2.89	−3.010	...	88	79
	5325.56	3.22	−3.170	73	66	65
	5414.04	3.22	−3.620	57	...	50
	5425.25	3.20	−3.210	71	71	63
	5534.83	3.25	−2.770	92	...	...
	5991.37	3.15	−3.560	65	57	51
	6084.09	3.20	−3.800	50	49	44
	6149.25	3.89	−2.720	60	57	51
	6247.55	3.89	−2.340	81	...	69
	6416.92	3.89	−2.680	65	57	54
	6432.68	2.89	−3.580	72	73	66

NGC 5822-2 and -201. Table 4 also shows the atmospheric parameters of HD 65314.

HD 2114 was included in our study after searching in the literature for a star with stellar parameters similar to those found for the cluster giants and with a spectrum that would be available in the ESO archives, so that a comparison between HD 2114 and the spectra of the stars studied here was possible. We obtained the following atmospheric parameters using the spectroscopic data from ESO: $T_{\rm eff} = 5200$, $\log g = 2.3$, $[{\rm Fe/H}] = -0.13$, and $\xi = 1.7$. These are similar to those found by Hekker & Meléndez (2007): $T_{\rm eff} = 5160$, $\log g = 2.55$, $[{\rm Fe/H}] = -0.15$, and $\xi = 1.85$.

The internal errors in our adopted effective temperatures ($T_{\rm eff}$) and microturbulent velocities (ξ) can be determined from the uncertainty in the slopes of the Fe I abundance versus excitation potential and Fe I abundance versus reduced equivalent width (W_λ/λ). The standard deviation in $\log g$ was set by changing this parameter around the adopted solution until the difference between the Fe I and Fe II mean abundance differed by exactly one standard deviation of the [Fe I/H] mean value. Based on the above description, we estimate typical uncertainties in atmospheric parameters of the order of ±100 K, ±0.20 dex, and ±0.2 km s^{-1} for $T_{\rm eff}$, $\log g$, and ξ, respectively.

To test our gravities obtained from spectroscopy for NGC 5822-2 and -201, we have calculated evolutionary

Table 3
Other Lines Studied

λ (Å)	Element	χ (eV)	log *gf*	Ref.	EQW_2 (mÅ)	EQW_{201} (mÅ)	EQW_{65314} (mÅ)
6154.22	Na I	2.10	−1.510	R03	72	71	67
6160.75	Na I	2.10	−1.210	R03	84	94	83
4730.04	Mg I	4.34	−2.390	R03	90	...	...
5711.10	Mg I	4.34	−1.750	R99	126	116	118
6318.71	Mg I	5.11	−1.940	Ca07	45	63	54
6319.24	Mg I	5.11	−2.160	Ca07	32	38	29
6319.49	Mg I	5.11	−2.670	Ca07	...	...	17
6765.45	Mg I	5.75	−1.940	MR94	26	...	...
6965.41	Mg I	5.75	−1.720	MR94	46	50	40
7387.70	Mg I	5.75	−0.870	MR94	...	...	69
8712.69	Mg I	5.93	−1.260	E93	52	51	51
8717.83	Mg I	5.91	−0.970	WSM	94	...	85
8736.04	Mg I	5.94	−0.340	WSM	128	145	...
6696.03	Al I	3.14	−1.481	MR94	48	...	48
6698.67	Al I	3.14	−1.630	R03	39	36	...
7835.32	Al I	4.04	−0.580	R03	56	64	56
7836.13	Al I	4.02	−0.400	R03	62	66	68
8772.88	Al I	4.02	−0.250	R03	...	102	90
8773.91	Al I	4.02	−0.070	R03	...	...	99
5793.08	Si I	4.93	−2.060	R03	71	60	57
6125.03	Si I	5.61	−1.540	E93	42	47	46
6131.58	Si I	5.62	−1.685	E93	35	33	30
6145.02	Si I	5.61	−1.430	E93	57	...	86
6155.14	Si I	5.62	−0.770	E93	91	102	86
7760.64	Si I	6.20	−1.280	E93	32	39	22
7800.00	Si I	6.18	−0.720	E93	67	78	70
8728.01	Si I	6.18	−0.360	E93	...	...	91
8742.45	Si I	5.87	−0.510	E93	110	113	...
5581.98	Ca I	2.52	−0.670	C2003	...	...	119
5867.57	Ca I	2.93	−1.610	C2003	...	...	37
6102.73	Ca I	1.88	−0.790	D2002	154	149	...
6161.30	Ca I	2.52	−1.270	E93	...	...	86
6166.44	Ca I	2.52	−1.140	R03	97	98	93
6169.04	Ca I	2.52	−0.800	R03	120	107	109
6169.56	Ca I	2.53	−0.480	DS91	128	134	...
6449.82	Ca I	2.52	−0.500	C2003	...	...	116
6455.60	Ca I	2.51	−1.290	R03	89	98	83
6464.68	Ca I	2.52	−2.410	C2003	...	...	30
6471.66	Ca I	2.51	−0.690	S86	121	116	112
6493.79	Ca I	2.52	−0.110	DS91	...	149	...
6499.65	Ca I	2.52	−0.810	C2003	...	...	105
6798.47	Ca I	2.71	−2.520	C2003	...	...	15
4512.74	Ti I	0.84	−0.480	MFK	114	...	...
4518.03	Ti I	0.83	−0.320	MFK	111	...	...
4534.78	Ti I	0.84	+0.280	MFK	139	...	...
4548.77	Ti I	0.83	−0.350	MFK	108	100	...
4555.49	Ti I	0.85	−0.489	MFK	98	105	...
4562.64	Ti I	0.02	−2.660	MFK	51	42	...
4617.28	Ti I	1.75	+0.389	MFK	102	95	...
4639.95	Ti I	1.74	−0.190	MFK	...	76	...
4681.92	Ti I	0.05	−1.070	MFK	...	114	...
4758.12	Ti I	2.25	+0.420	MFK	64	...	65
4759.28	Ti I	2.25	+0.511	MFK	71	72	69
4778.26	Ti I	2.24	−0.300	MFK	35	36	...
4997.10	Ti I	0.00	−2.120	MFK	72	67	...
5009.66	Ti I	0.02	−2.259	MFK	...	...	71
5016.17	Ti I	0.85	−0.570	MFK	116	100	100
5022.87	Ti I	0.83	−0.429	MFK	115	111	106
5039.96	Ti I	0.02	−1.130	MFK	...	...	117
5040.61	Ti I	0.83	−1.787	MFK	...	...	50
5043.59	Ti I	0.84	−1.733	MFK	...	...	49
5062.10	Ti I	2.16	−0.460	MFK	37	34	33
5087.06	Ti I	1.43	−0.840	MFK	...	...	66
5113.45	Ti I	1.44	−0.780	E93	51	50	52
5145.47	Ti I	1.46	−0.570	MFK	78	67	65

Table 3
(Continued)

λ (Å)	Element	χ (eV)	log *gf*	Ref.	EQW_2 (mÅ)	EQW_{201} (mÅ)	EQW_{65314} (mÅ)
5147.48	Ti I	0.00	−2.012	MFK	...	...	91
5152.19	Ti I	0.02	−0.202	MFK	78	70	...
5210.39	Ti I	0.05	−0.879	MFK	148	143	...
5219.71	Ti I	0.02	−2.290	MFK	80	73	73
5223.63	Ti I	2.09	−0.561	MFK	27	42	37
5282.44	Ti I	1.05	−1.300	MFK	55	48	...
5295.78	Ti I	1.05	−1.631	MFK	36	29	38
5490.16	Ti I	1.46	−0.932	MFK	49	47	47
5503.90	Ti I	2.58	−0.190	MFK	...	20	...
5662.16	Ti I	2.32	−0.110	MFK	54	...	47
5689.48	Ti I	2.30	−0.470	MFK	35	28	32
5866.46	Ti I	1.07	−0.871	E93	...	...	90
5922.12	Ti I	1.05	−1.470	MFK	65	44	51
5978.55	Ti I	1.87	−0.500	MFK	52	51	54
6091.18	Ti I	2.27	−0.370	R03	44	...	32
6126.22	Ti I	1.05	−1.420	R03	71	64	61
6258.11	Ti I	1.44	−0.360	MFK	100	90	85
6261.10	Ti I	1.43	−0.480	B86	94	82	91
6554.24	Ti I	1.44	−1.220	MFK	42	43	40
4836.85	Cr I	3.10	−1.140	MFK	...	33	...
4936.34	Cr I	3.11	−0.220	MFK	68	67	...
4954.80	Cr I	3.12	−0.140	MFK	...	69	...
4964.93	Cr I	0.94	−2.526	MFK	...	...	68
5193.50	Cr I	3.42	−0.900	MFK	29	...	19
5214.13	Cr I	3.37	−0.740	MFK	25	27	25
5214.61	Cr I	3.32	−0.660	MFK	44	49	...
5238.96	Cr I	2.71	−1.300	MFK	29	34	31
5247.57	Cr I	0.96	−1.631	MFK	132	121	111
5272.00	Cr I	3.45	−0.420	MFK	36	35	40
5296.70	Cr I	0.98	−1.240	GS	143	135	...
5298.28	Cr I	0.98	−1.170	MFK	...	144	...
5300.75	Cr I	0.98	−2.130	GS	97	97	90
5304.18	Cr I	3.46	−0.690	MFK	26	27	23
5312.86	Cr I	3.45	−0.561	MFK	44	30	25
5318.77	Cr I	3.44	−0.690	MFK	27	31	21
5340.45	Cr I	3.44	−0.730	MFK	20	...	26
5348.33	Cr I	1.00	−1.290	GS	145	125	...
5628.65	Cr I	3.42	−0.770	MFK	21	29	20
5781.18	Cr I	3.32	−0.879	MFK	26	...	...
5783.07	Cr I	3.32	−0.400	MFK	48	52	42
5784.97	Cr I	3.32	−0.380	MFK	48	47	48
5787.93	Cr I	3.32	−0.080	GS	72	68	63
6330.10	Cr I	0.94	−2.870	R03	70	68	64
4513.00	Ni I	3.71	−1.520	MFK	...	30	...
4904.42	Ni I	3.54	−0.190	MFK	...	105	100
4913.98	Ni I	3.74	−0.600	MFK	76	78	72
4935.83	Ni I	3.94	−0.340	MFK	83	...	64
4953.21	Ni I	3.74	−0.620	MFK	...	80	75
4967.52	Ni I	3.80	−1.600	MFK	25	31	28
4995.66	Ni I	3.63	−1.611	MFK	38	35	33
5003.75	Ni I	1.68	−3.130	MFK	65	64	...
5010.94	Ni I	3.63	−0.900	MFK	72	62	62
5084.11	Ni I	3.68	−0.180	E93	...	...	98
5094.42	Ni I	3.83	−1.120	MFK	47	45	41
5115.40	Ni I	3.83	−0.280	R03	...	...	87
5157.98	Ni I	3.61	−1.720	MFK	35	37	29
5197.17	Ni I	3.90	−1.140	MFK	48	46	43
5578.73	Ni I	1.68	−2.640	MFK	...	...	95
5587.87	Ni I	1.94	−2.370	MFK	99	90	...
5589.37	Ni I	3.90	−1.150	MFK	38	...	34
5593.75	Ni I	3.90	−0.790	MFK	62	72	55
5643.09	Ni I	4.17	−1.250	MFK	31	28	22
5709.56	Ni I	1.68	−2.140	MFK	...	110	111
5748.36	Ni I	1.68	−3.250	MFK	66	68	64
5760.84	Ni I	4.11	−0.810	MFK	56	61	47

Table 3
(Continued)

λ (Å)	Element	χ (eV)	log gf	Ref.	EQW_2 (mÅ)	EQW_{201} (mÅ)	EQW_{65314} (mÅ)
5805.23	Ni I	4.17	−0.600	MFK	56	54	49
5847.01	Ni I	1.68	−3.440	MFK	60	51	. . .
5996.74	Ni I	4.24	−1.060	MFK	39	37	31
6053.69	Ni I	4.24	−1.070	MFK	42	. . .	32
6086.29	Ni I	4.27	−0.470	MFK	58	68	58
6108.12	Ni I	1.68	−2.440	MFK	. . .	. . .	100
6111.08	Ni I	4.09	−0.830	MFK	54	54	48
6128.98	Ni I	1.68	−3.390	MFK	68	65	57
6130.14	Ni I	4.27	−0.979	MFK	40	37	31
6176.82	Ni I	4.09	−0.260	MFK	86	88	78
6177.25	Ni I	1.83	−0.360	MFK	38	39	35
6186.72	Ni I	4.11	−0.900	MFK	43	42	38
6204.61	Ni I	4.09	−1.150	MFK	. . .	37	38
6223.99	Ni I	4.11	−0.971	MFK	53	. . .	41
6230.10	Ni I	4.11	−1.200	MFK	42	41	. . .
6322.17	Ni I	4.15	−1.210	MFK	30	25	27
6327.60	Ni I	1.68	−3.090	MFK	86	86	74
6378.26	Ni I	4.15	−0.821	MFK	55	. . .	49
6384.67	Ni I	4.15	−1.000	MFK	. . .	44	35
6482.81	Ni I	1.94	−2.851	MFK	86	84	73
6532.88	Ni I	1.94	−3.420	MFK	. . .	48	37
6586.33	Ni I	1.95	−2.790	MFK	78	75	76
6598.61	Ni I	4.24	−0.932	MFK	40	41	. . .
6635.14	Ni I	4.42	−0.750	MFK	48	. . .	38
6643.64	Ni I	1.68	−2.030	MFK	146	. . .	. . .
6767.77	Ni I	1.83	−2.110	MFK	131	123	116
6772.32	Ni I	3.66	−1.010	R03	. . .	75	69
6842.04	Ni I	3.66	−1.440	MFK	47	40	41
7788.93	Ni I	1.95	−1.990	E93	148	. . .	. . .
4883.68	Y II	1.08	+0.070	SN96	. . .	144	. . .
5087.43	Y II	1.08	−0.170	SN96	120	126	107
5123.21	Y II	0.99	−0.930	SN96	. . .	92	. . .
5200.41	Y II	0.99	−0.570	SN96	124	112	100
5205.72	Y II	1.03	−0.340	SN96	141	116	. . .
5289.81	Y II	1.03	−1.850	VWR	59	52	45
5402.78	Y II	1.84	−0.440	R03	91	76	60
4772.30	Zr I	0.62	−0.060	A05	49	50	37
4784.94	Zr I	0.69	−0.600	A05	. . .	. . .	17
4805.87	Zr I	0.69	−0.580	A05	19	17	16
4809.47	Zr I	1.58	+0.350	A05	14	15	10
4815.05	Zr I	0.65	−0.380	A05	. . .	. . .	17
4815.63	Zr I	0.60	−0.270	A05	. . .	33	27
4828.05	Zr I	0.62	−0.750	A05	. . .	18	10
5385.13	Zr I	0.52	−0.640	A05	20	23	18
5879.79	Zr I	0.15	−1.030	A05	27	26	17
5955.34	Zr I	0.00	−1.700	A05	. . .	17	. . .
6127.46	Zr I	0.15	−1.060	S96	15	30	27
6134.57	Zr I	0.00	−1.280	S96	15	31	26
6143.18	Zr I	0.07	−1.100	S96	15	32	34
4086.71	La II	0.00	−0.160	VWR	110	. . .	. . .
5122.99	La II	0.32	−0.930	SN96	. . .	68	. . .
5303.53	La II	0.32	−1.350	VWR	49	52	45
5880.63	La II	0.24	−1.830	R04	31	. . .	39
6320.42	La II	0.17	−1.520	VWR	55	61	49
6390.48	La II	0.32	−1.410	SN96	62	46	50
6774.33	La II	0.12	−1.709	SN96	58	56	51
4073.47	Ce II	0.48	+0.320	SN96	91	. . .	. . .
4120.84	Ce II	0.32	−0.240	SN96	74	. . .	. . .
4127.38	Ce II	0.68	+0.240	SN96	82	78	. . .
4418.79	Ce II	0.86	+0.310	SN96	83	. . .	77
4486.91	Ce II	0.30	−0.360	SN96	. . .	. . .	78
4562.37	Ce II	0.48	+0.330	SN96	98	95	94
4628.16	Ce II	1.40	+0.010	SN96	. . .	. . .	93
5117.17	Ce II	1.40	+0.010	VWR	36	29	38
5187.45	Ce II	1.21	+0.300	VWR	59	51	. . .
5274.24	Ce II	1.28	+0.389	VWR	61	. . .	57
5472.30	Ce II	1.25	−0.190	VWR	44	35	39
6051.80	Ce II	0.23	−1.600	SN96	. . .	22	30
4811.34	Nd II	0.06	−1.015	VWR	73	70	78
4959.12	Nd II	0.06	−0.916	VWR	. . .	. . .	83
5063.72	Nd II	0.98	−0.758	VWR	. . .	32	28
5130.59	Nd II	1.30	+0.100	SN96	59	62	62
5212.36	Nd II	0.20	−0.700	E93	85	. . .	. . .
5234.19	Nd II	0.55	−0.460	SN96	. . .	59	. . .
5311.46	Nd II	0.99	−0.560	SN96	52	49	46
5319.81	Nd II	0.55	−0.350	SN96	87	78	74
5416.38	Nd II	0.86	−0.980	VWR	18	. . .	. . .
5431.54	Nd II	1.12	−0.457	VWR	34	37	. . .
5442.26	Nd II	0.68	−0.900	SN96	. . .	47	. . .
5740.88	Nd II	1.16	−0.560	VWR	28	. . .	. . .
5842.39	Nd II	1.28	−0.601	VWR	20	. . .	. . .

References. A05: Antipova et al. 2005; B86: Blackwell et al. 1986; Ca07: Carretta et al. 2007; C2003: Chen et al. 2003; D2002: Depagne et al. 2002; DS91: Drake & Smith 1991; E93: Edvardsson et al. 1993; GS: Gratton & Sneden 1988; MFK: Martin et al. 1999; MR94: McWilliam & Rich 1994; R03: Reddy et al. 2003; R04: Reyniers et al. 2004; R99: Reddy et al. 1999; S86: Smith et al. 1986; S96: Smith et al. 1996; SN96: Sneden et al. 1996; VWR: van Winckel & Reyniers 2000; WSM: Wiese et al. 1969.

gravities from the equation below:

$$\log g_\star = \log(M_\star/M_\odot) + 0.4(V - A_v + BC) + 4\log T_{\rm eff} - 2\log r(\mathrm{kpc}) - 16.5. \quad (1)$$

The turnoff mass ($M = 2.1\,M_\odot$), interstellar absorption ($A_V = 0.45$), and distance ($r = 697$ pc) for NGC 5822 were taken from Table 2 of Smiljanic et al. (2009), and bolometric corrections were taken from Alonso et al. (1999). We found a mean difference of approximately of 0.1 dex for both stars between the spectroscopic and evolutionary gravities.

3.3. Abundance Analysis

The abundances of chemical elements were determined with LTE model atmosphere techniques. The equivalent widths were calculated by integration through a model atmosphere and were compared with the measured equivalent widths. The current version of the line-synthesis code MOOG (Sneden 1973) was used to carry out the calculations. Table 5 shows the derived abundances of the elements and also the number of lines employed (or number of spectral regions, in the case of carbon and nitrogen whose abundances were determined using molecular lines) for each species, n, the standard deviation, and in the notations [X/H] and [X/Fe] as well as the C/O ratio. The adopted abundances for the elements analyzed in this work were normalized to the solar abundances of Grevesse & Sauval (1998). For the solar iron abundance, we adopted log ε(Fe) = 7.52.

Carbon, nitrogen, and oxygen abundances were determined using the spectrum synthesis technique. For the oxygen abundance in NGC 5822-2 and -201, we used the line at 6363.78 Å because the line at 6300.31 Å is contaminated by the telluric O_2 line in both stars. The gf value for the 6363.78 Å line was taken from Lambert (1978). In HD 65314, we used the forbidden line at 6300.63 Å to obtain the oxygen abundance.

Table 4
Atmospheric Parameters of NGC 5822-2 and -201 and the Barium star HD 65314

	NGC 5822-2	NGC 5822-201	NGC 5822-2[a]	NGC 5822-201[b]	HD 65314
$T_{\rm eff}$ (K)	5100 ± 100	5200 ± 120	5100	5035	5000 ± 120
log g (dex)	2.4 ± 0.2	2.7 ± 0.2	2.25	2.85	2.5 ± 0.2
[Fe/H] (dex)	−0.15 ± 0.09	−0.11 ± 0.10	0.04	0.05 ± 0.10	−0.12 ± 0.11
ξ (km s^{-1})	1.6 ± 0.2	1.5 ± 0.2	2.2	1.32	1.2 ± 0.3

Notes.
[a] Luck (1994).
[b] Smiljanic et al. (2009).

Table 5
Abundances in the log ε(H) = 12.0 Scale and in the Notations [X/H] and [X/Fe]

Species	NGC 5822-2				NGC 5822-201				HD 65314			
	n	log ε	[X/H]	[X/Fe]	n	log ε	[X/H]	[X/Fe]	n	log ε	[X/H]	[X/Fe]
Fe I	57	7.37 ± 0.09	−0.15	...	66	7.41 ± 0.10	−0.11	...	72	7.39 ± 0.11	−0.13	...
Fe II	13	7.37 ± 0.06	−0.15	...	11	7.41 ± 0.09	−0.11	...	13	7.39 ± 0.08	−0.13	...
C I	2	8.30	−0.22	−0.07	2	8.52	0.00	+0.11	2	8.32	−0.20	−0.07
N I	6	8.39 ± 0.08	+0.47	+0.62	6	8.35 ± 0.09	+0.43	+0.54	6	8.27 ± 0.07	+0.35	+0.46
O I	1	8.53	−0.30	−0.15	1	8.82	−0.01	+0.10	1	8.53	−0.30	−0.17
Na I	2	6.37	+0.04	+0.19	2	6.29	−0.04	+0.07	2	6.31	−0.02	+0.11
Mg I	7	7.66 ± 0.10	+0.08	+0.23	8	7.61 ± 0.15	+0.03	+0.14	8	7.46 ± 0.17	−0.12	−0.01
Al I	4	6.29 ± 0.07	−0.18	−0.03	4	6.52 ± 0.12	+0.05	+0.16	5	6.39 ± 0.11	−0.06	+0.07
Si I	8	7.59 ± 0.09	+0.04	+0.19	5	7.65 ± 0.11	+0.10	+0.21	8	7.55 ± 0.12	0.00	−0.13
Ca I	8	6.33 ± 0.08	−0.03	+0.12	5	6.34 ± 0.07	−0.02	+0.09	11	6.26 ± 0.10	−0.10	+0.03
Ti I	27	4.86 ± 0.11	−0.16	−0.01	32	4.88 ± 0.13	−0.14	−0.03	27	4.71 ± 0.09	−0.31	−0.19
Cr I	20	5.51 ± 0.13	−0.16	−0.01	20	5.59 ± 0.11	−0.08	0.03	16	5.35 ± 0.07	−0.32	−0.19
Ni I	38	6.14 ± 0.09	−0.11	+0.04	40	6.20 ± 0.10	−0.05	+0.06	43	6.06 ± 0.11	−0.19	−0.06
Y II	4	3.02 ± 0.13	+0.78	+0.93	6	2.96 ± 0.10	+0.72	+0.83	4	2.72 ± 0.11	+0.48	+0.61
Zr I	8	3.05 ± 0.08	+0.45	+0.60	11	3.24 ± 0.09	+0.64	+0.75	12	2.83 ± 0.12	+0.23	+0.36
La II	6	1.77 ± 0.12	+0.60	+0.75	5	1.94 ± 0.06	+0.77	+0.88	5	1.80 ± 0.09	+0.63	+0.76
Ce II	10	2.18 ± 0.13	+0.60	+0.75	5	2.36 ± 0.16	+0.76	+0.87	8	2.4 ± 0.22	+0.82	+0.95
Nd II	8	2.15 ± 0.16	+0.65	+0.80	10	2.20 ± 0.15	+0.70	+0.81	6	2.38 ± 0.19	+0.88	+1.01
	C/O = 0.59				C/O = 0.50				C/O = 0.61			

Since the abundances of the CNO elements are interdependent because of the association of carbon and oxygen in CO molecules in the atmospheres of cool giants, the CNO abundance determination procedure was iterated until all the abundances of these three elements agreed. The abundances of carbon and nitrogen were determined using the lines of the CN and C_2 molecules. The line lists used in this work are the same as used in previous studies done for some barium stars (Pereira & Drake 2009; Drake & Pereira 2011). The observed and synthetic spectra of NGC 5822-2, -201, and HD 65314 in the region around the C_2 molecule at 5635 Å are shown in Figure 5.

We do not measure the barium abundance in our stars because all barium lines have equivalent widths higher than 200 mÅ and therefore will not be at the linear part of the curve of growth (Hill et al. 1995; Pereira et al. 2011). However, since we have measured several other lines of other elements synthesized by the *s*-process (Y, Zr, La, Ce, and Nd), we believe that we probed this nucleosynthesis process in NGC 5822-2 and NGC 5822-201 fairly well.

3.4. Abundance Uncertainties

The abundance uncertainties of NGC 5822-2 and -201 are shown in Tables 6 and 7. HD 65314 also displays similar abundance uncertainties. The abundance uncertainties due to the errors in the effective temperatures and microturbulent velocities were determined by changing these parameters around the adopted solutions until the difference in the iron abundance became one standard deviation. The uncertainties in the abundances, due to errors in the stellar atmospheric parameters, were computed by changing these parameters by their standard deviations given in Table 4 and calculating the changes incurred in the element abundances. The final uncertainty of the abundance by number is found by composing quadratically the uncertainties due to atmospheric parameters and the W_λ's. The abundance uncertainties resulting from the errors in the equivalent width measurements were computed from the expression provided by Cayrel (1988). These errors we are set, essentially, by the S/N and the resolution of the spectra. In our case, having 48,000 and a typical S/N of 150, the expected uncertainties in the equivalent widths are about 2–3 mÅ. For all measured equivalent widths, these uncertainties led to errors in the abundances less than those due to the uncertainties in the stellar parameters. They were calculated by quadratically combining the different sources of errors under the assumption that the errors were independent. In the last column of Tables 6 and 7, we quote the observed abundance dispersion among the lines for those elements with more than three available lines.

We verify the well-known relations from Tables 6 and 7 that neutral elements are more sensitive to the temperature variations, while singly ionized elements are more sensitive to the variations in log g. For the elements whose abundance is

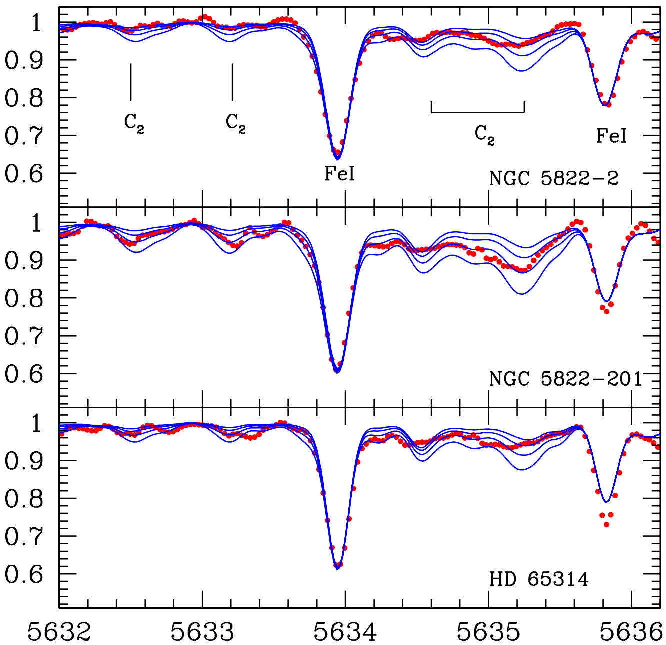

Figure 5. Observed (dotted red line) and synthetic (solid blue line) spectra in the region around the C_2 molecule lines at 5635 Å for the stars NGC 5822-2, NGC 5822-201, and HD 65314. In the synthetic spectra of NGC 5822-2, we show the synthesis for carbon abundances of $\log \varepsilon(\mathrm{C}) = 8.20$, 8.30, 8.40, and 8.52; for NGC 5822-201, we show the synthesis for carbon abundances of $\log\varepsilon(\mathrm{C}) = 8.32$, 8.42, 8.52, and 8.62; and for HD 65314, we show the synthesis for carbon abundances of $\log \varepsilon(\mathrm{C}) = 8.12$, 8.22, 8.32, and 8.42.

based on stronger lines, such as the lines of calcium, yttrium, and cerium, the error introduced by the microturbulence is important.

4. DISCUSSION

4.1. Luminosities of NGC 5822-2 and NGC 5822-201

For NGC 5822-2 and -201, the bolometric magnitude which results from the adopted turnoff mass, temperature, and gravity of the two stars is, respectively, $M_{\mathrm{bol}\star} = -0.6 \pm 0.5$ (with a luminosity of 140 $L_\odot$) and $M_{\mathrm{bol}\star} = 0.0 \pm 0.5$ (with luminosity of 76 $L_\odot$), assuming $M_{\mathrm{bol}\odot} = +4.74$ for the Sun (Bessel et al. 1998). These luminosities are too low to consider NGC 5822-2 and -201 as AGB stars that started shell helium burning (via thermal pulses) and became self-enriched in the neutron-capture elements. In fact, theoretical calculations show that in order to develop the first thermal pulse, the star's luminosity should be $\simeq$1800 $L_\odot$ ($M_{\mathrm{bol}} = -3.4$; Lattanzio 1986) or $\simeq$1400 $L_\odot$ ($M_{\mathrm{bol}} = -3.1$; Vassiliadis & Wood, 1993).

Since we know the distance of the cluster of NGC 5822, we can also compare the masses of these giants with the masses of the field barium stars. The masses of barium stars have already been determined in the literature. The determinations were made either by the available parallax or by placing them in $\log g$–$\log T_{\mathrm{eff}}$ diagram with theoretical evolutionary tracks (Allen & Barbuy 2006; Antipova et al. 2003, 2004; Boyarchuk et al. 2002; Liang et al. 2003; Pereira et al. 2011; Smiljanic et al. 2007). In all these studies, the authors found that the masses of barium stars are in the range between 1.3 and 4.2 $M_\odot$. To date, the most complete analysis of the determination of the mass of barium stars is the work of Mennesier et al. (1997). There, the authors, using the *Hipparcos* parallaxes and based on the Lu (1991) catalog, showed from the absolute magnitude versus intrinsic color index diagram that the mass of barium stars is in the range between 1.25 and 7.0 $M_\odot$. However, some high values found for the mass of some barium stars should be viewed with caution since there are many stars in the Lu (1991) catalog that are not barium stars. As far as the two giants in NGC 5822 are concerned, their masses are also constrained by the cluster age and the turnoff mass. With a value of 2.1 $M_\odot$, (Section 3.2), we can see that they also lie in the same range of the field barium stars.

Table 6
Abundance Uncertainties of NGC 5822-2

Species	ΔT_{eff}	$\Delta \log g$ +100 K	$\Delta\xi$ +0.2	ΔW_λ +0.2	$\left(\sum \sigma^2\right)^{1/2}$ +3 mÅ	σ_{obs}
Fe I	−0.09	+0.00	+0.08	−0.06	0.13	0.09
Fe II	−0.06	−0.07	+0.08	−0.07	0.14	0.06
C I	−0.01	+0.04	−0.04	...	0.06	...
N I	−0.10	+0.06	+0.09	...	0.15	0.08
O I	−0.02	−0.10	−0.01	...	0.10	...
Na I	−0.06	+0.01	+0.04	−0.04	0.08	...
Mg I	−0.04	+0.01	+0.04	−0.04	0.07	0.10
Al I	−0.05	+0.00	+0.02	−0.05	0.07	0.07
Si I	0.00	−0.02	+0.03	−0.05	0.06	0.09
Ca I	−0.10	+0.01	+0.11	−0.05	0.15	0.08
Ti I	−0.13	+0.00	+0.08	−0.06	0.16	0.11
Cr I	−0.09	+0.01	+0.06	−0.06	0.12	0.13
Ni I	−0.07	−0.01	+0.06	−0.06	0.11	0.09
Y II	0.00	−0.06	+0.15	−0.06	0.17	0.13
Zr I	−0.15	+0.00	+0.01	−0.07	0.17	0.08
La II	−0.02	−0.07	+0.07	−0.06	0.12	0.12
Ce II	−0.01	−0.06	+0.14	−0.07	0.17	0.13
Nd II	−0.02	−0.07	+0.09	−0.07	0.14	0.16

Notes. Column 2 gives the variation of the abundance caused by the variation in T_{eff}. The other columns refer, respectively, to the variations due to $\log g$, ξ, and W_λ. Column 6 gives the compounded rms uncertainty of the second to fifth columns. The last column gives the observed abundance dispersion for those elements whose abundances were derived using more than three lines.

Table 7
Abundance Uncertainties of NGC 5822-201

Species	ΔT_{eff}	$\Delta \log g$ +120 K	$\Delta\xi$ +0.2	ΔW_λ +0.2	$\left(\sum \sigma^2\right)^{1/2}$ +3 mÅ	σ_{obs}
Fe I	−0.11	+0.00	+0.08	−0.06	0.15	0.10
Fe II	+0.06	−0.08	+0.08	−0.06	0.14	0.09
C I	−0.06	−0.03	−0.03	...	0.07	...
N I	−0.17	−0.04	−0.04	...	0.18	0.09
O I	−0.03	−0.08	−0.01	...	0.09	...
Na I	−0.08	+0.01	+0.03	−0.04	0.09	...
Mg I	−0.05	+0.01	+0.03	−0.05	0.08	0.15
Al I	−0.06	+0.01	+0.04	−0.05	0.09	0.12
Si I	−0.02	+0.00	+0.04	−0.05	0.07	0.11
Ca I	−0.11	+0.00	+0.12	−0.05	0.17	0.07
Ti I	−0.15	+0.01	+0.07	−0.06	0.18	0.13
Cr I	−0.12	−0.01	+0.07	−0.06	0.15	0.11
Ni I	−0.10	−0.02	+0.05	−0.06	0.13	0.10
Y II	−0.01	−0.04	+0.15	−0.06	0.18	0.10
Zr I	−0.17	−0.01	+0.01	−0.08	0.18	0.09
La II	−0.02	−0.05	+0.07	−0.06	0.11	0.06
Ce II	−0.03	−0.12	+0.16	−0.08	0.22	0.16
Nd II	−0.02	−0.14	+0.06	−0.07	0.17	0.15

Note. Columns and symbols have the same meaning as in Table 6.

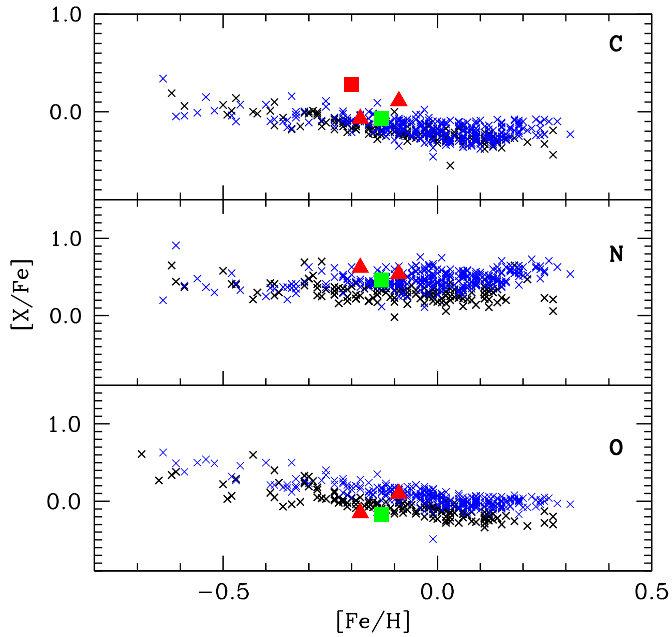

Figure 6. Chemical abundances of carbon, nitrogen, and oxygen given as a function of the metallicity for NGC 5822-2 and -201 (red triangles), NGC 2420-X (red square), and HD 65314 (green square). Blue crosses represent field giants of Luck & Heiter (2007), whereas black crosses the clump giants of Mishenina et al. (2006).

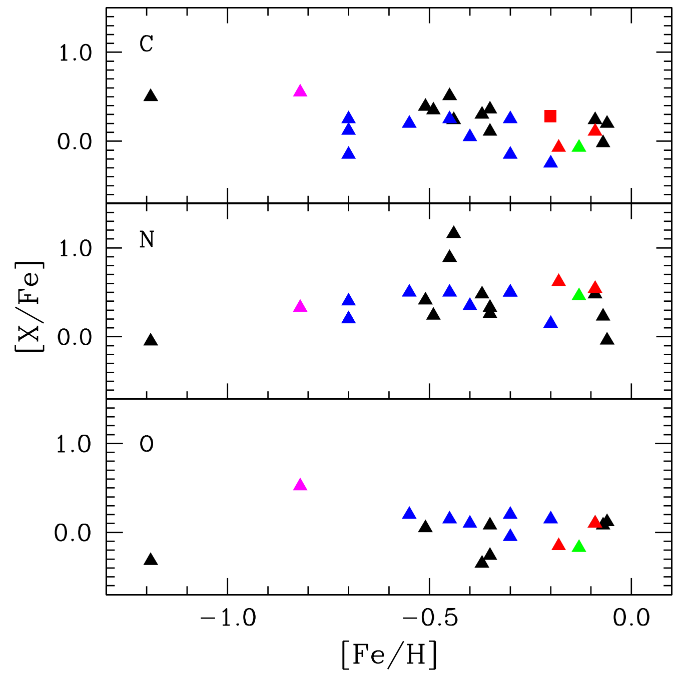

Figure 7. Chemical abundances of carbon, nitrogen, and oxygen given as a function of the metallicity for field barium stars from Barbuy et al. (1992, blue triangles), Allen & Barbuy (2006, black triangles), and the star HD 10613 from Pereira & Drake (2009, magenta triangle). Other symbols have the same meanings as in Figure 6 for the stars analyzed in this work and for NGC 2420-X.

4.2. Abundance Pattern

4.2.1. Carbon, Nitrogen, and Oxygen

In Figure 6, we compare our CNO abundances obtained for NGC 5822-2 and -201 and HD 65314 with field giant stars analyzed by Mishenina et al. (2006) and Luck & Heiter (2007). We also included the [C/Fe] ratio for another barium star in the open cluster NGC 2420 from Smith & Suntzeff (1987). The [C/Fe] and [N/Fe] ratios for the field giants were computed using absolute abundances on the scale of $\log \varepsilon(\mathrm{H}) = 12.0$ obtained in these papers and then converted to [X/Fe] ratios using the solar abundances adopted in this work (Section 3.3). As seen in Figure 6, the [N/Fe] ratios for these two cluster giants have similar values of the giants analyzed by Mishenina et al. (2006) and Luck & Heiter (2007). Figure 6 also shows that nitrogen is overabundant with respect to the Sun in field giants as well as in NGC 5822-2 and -201 and in HD 65314. As a star becomes giant, due to deepening of its convective envelope, nuclear processed material is brought from the interior to the outer layers of the star, which changes the surface composition. As a consequence of the first dredge-up process, the abundance of ^{12}C is reduced and the abundance of ^{14}N is enhanced (Lambert 1981). Our results for the [N/Fe] ratio show the effects of the first dredge-up.

We updated the metallicity of the two barium stars of NGC 2420 as well as the carbon and the heavy-element abundances. Smith & Suntzeff (1987) derived a metallicity of −0.55 and −0.68, respectively, for stars D and X. These observations were made at lower resolution and with a spectral coverage of 200 Å. As was discussed in Jacobson et al. (2011), NGC 2420 could be more metal-rich than −0.57, as was earlier derived by Smith & Suntzeff (1987). In fact, the authors obtained a mean metallicity of −0.20, which we adopted for stars X and D to obtain the [X/Fe] ratios ([C/Fe] and the [*s*-process/Fe]) seen in Figures 6, 7, 10, and 11.

The [O/Fe] ratios of NGC 5822-2 and -201 and HD 65314 are similar to those seen in field giants. The [O/Fe] ratio was also computed based on an absolute abundance and then converted to the [X/Fe] ratio using the solar abundances adopted in Section 3.3. For this reason, there is an offset of −0.13 dex in the [O/Fe] ratio between Figure 6 in this paper and Figure 13 in Mishenina et al. (2006), who adopted a solar oxygen abundance of 8.70. Luck & Heiter (2007) adopted a solar oxygen abundance (8.81) similar to this paper's, and because of that our normalized [O/Fe] ratio is equal to the ratio derived by these authors.

Figure 7 shows the CNO abundances of our target stars with some previous determinations done for some barium giant stars (Barbuy et al. 1992; Allen & Barbuy 2006; Pereira & Drake 2009). Our derived [C/Fe] ratios are in good agreement with these previous analyses. The barium stars also shown the effects of the first dredge-up episode, since we also observed nitrogen enrichment. As far as oxygen is concerned, our [O/Fe] is also in agreement with these previous determinations in the barium giants.

4.2.2. Other Elements: Na to Ni

Sodium and aluminum, α-elements (Mg, Si, Ca, and Ti), and iron-peak elements (Cr and Ni) in NGC 5822-2 and -201 as well as in HD 65314 follow the general trend seen in the field giants analyzed by Luck & Heiter (2007). Figures 8 and 9 show the abundances of the above-mentioned elements for our studied stars.

4.2.3. Heavy Elements: Neutron-capture Elements

Figure 10 shows the abundances of Y, La, Ce, and Nd for NGC 5822-2 and -201 as well as for the barium stars HD 65314 and NGC 2420-X and D (Smith & Suntzeff 1987). Clearly, these stars have higher abundances of these elements

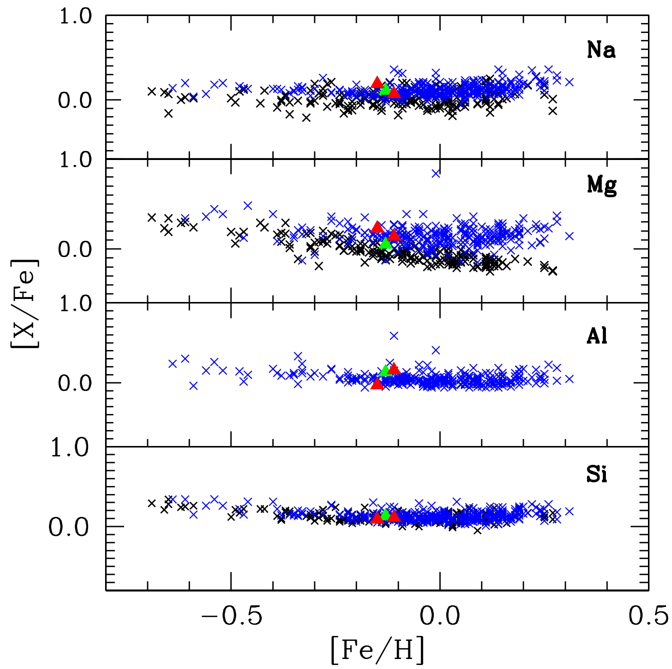

Figure 8. Abundance ratios [X/Fe] vs. [Fe/H]. Symbols have the same meanings as in Figure 6.

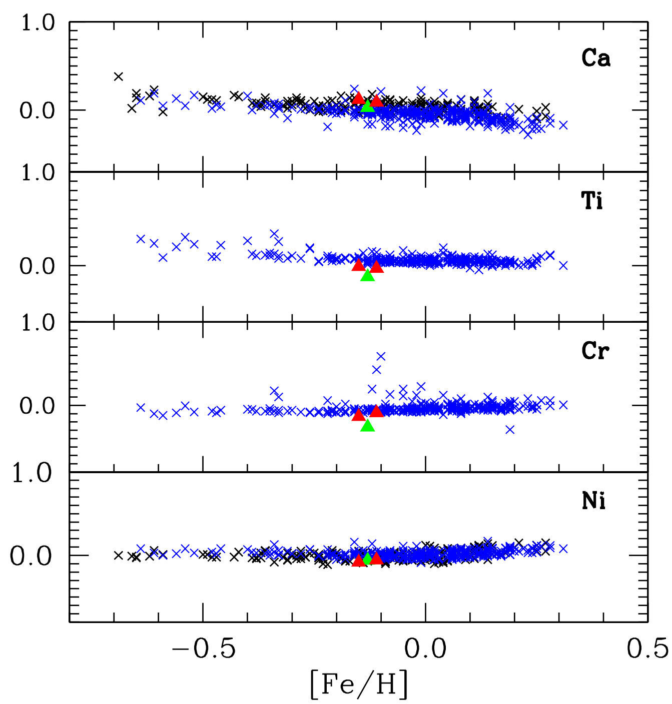

Figure 9. Abundance ratios [X/Fe] vs. [Fe/H]. Symbols have the same meaning as in Figure 6.

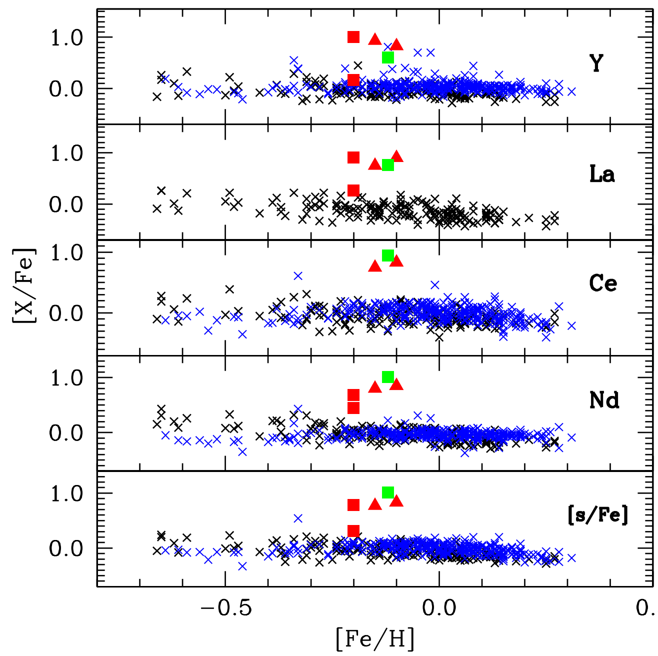

Figure 10. Abundance ratios [X/Fe] vs. [Fe/H]. Symbols have the same meaning as in Figure 6 (red squares represent NGC 2420-X and -D). Among the local giants analyzed by Luck & Heiter (2007), only one barium star was spotted, HD 104979 (Začs 1994), which can be seen at [Fe/H] = −0.33 with [s/Fe] = +0.54.

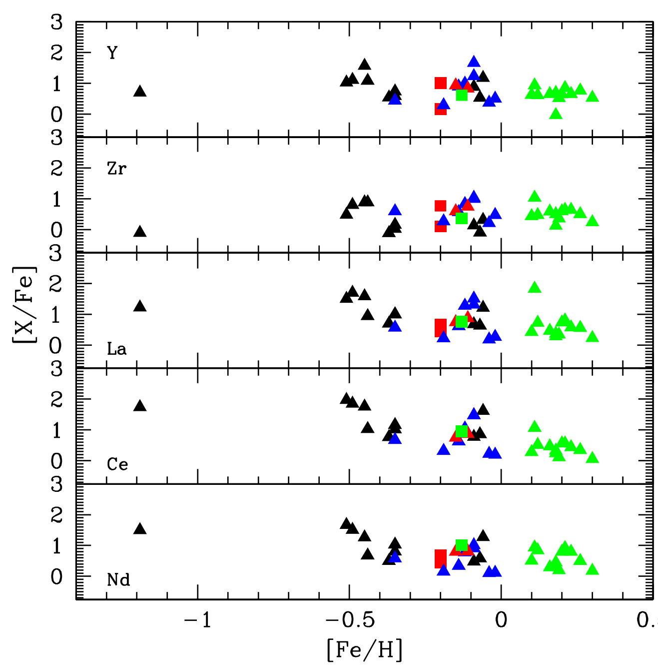

Figure 11. Abundance ratios [X/Fe] vs. [Fe/H] for field barium stars as a function of metallicity from Allen & Barbuy (2006, black triangles), Pereira et al. (2011, green triangles), and Smiljanic et al. (2007, blue triangles). Red squares represent the barium giants in NGC 2420. Green squares represent HD 65314 and red triangles represent NGC 5822-2 and -201.

than field giants. This result is interesting because these differences are significant for the four elements. This fact is also noted at the bottom of Figure 10, where we also provide the *mean* abundance of these heavy elements, "s" in the notation [s/Fe]. We obtained [s/Fe] = 0.77 ± 0.12 and 0.83 ± 0.05, respectively, for NGC 5822-2 and -201. These values are not only much higher than the mean value for the field giants at similar metallicity ([s/Fe] ≈ 0.1 and [s/Fe] = 0.17 ± 0.12 for HD 2114), but also it is similar to the values found in other barium stars (as can be seen in Figure 11). For the barium star HD 65314, we have [s/Fe] = 0.74 ± 0.4. The abundance of zirconium (not shown in the figure) was also taken into account to calculate [s/Fe]; however, in the literature there are not many results for the zirconium abundance in field giants, except for barium stars (Antipova et al. 2005; Allen & Barbuy 2006; Smiljanic et al. 2007; Pereira et al. 2011).

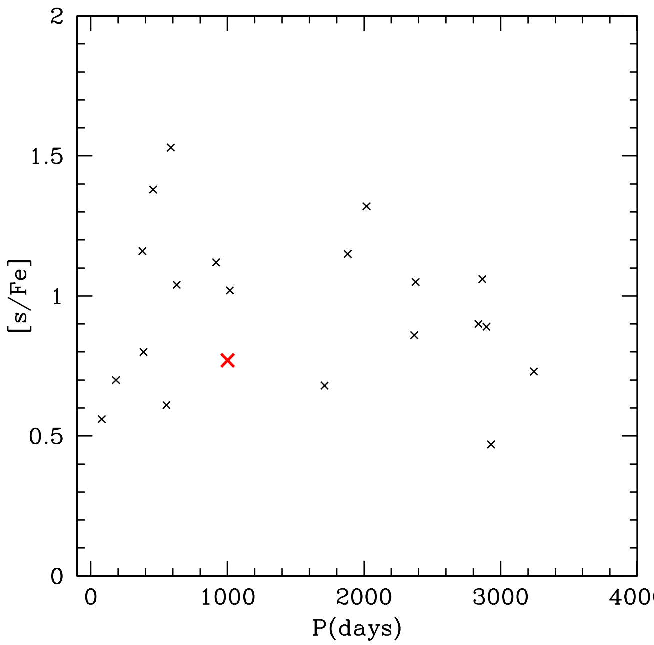

Figure 12. Relationship between the orbital period and *mean* *s*-process abundance of NGC 5822-2 (red cross) in comparison with a sample of field barium stars (black crosses). Orbital periods were taken from Jorissen et al. (1998). Heavy element abundances were taken from Allen & Barbuy (2006), Antipova et al. (2003, 2004), Kovacs (1985), Liang et al. (2003), Liu et al. (2009), Masseron et al. (2010), Smiljanic et al. (2007), Smith (1984), and Začs (1994).

In Figure 12, we show the relationship between the orbital period and the [*s*/Fe] for a sample of field barium stars. We used the available period data from Jorissen et al. (1998) and the [*s*/Fe] ratios from different sources of the literature. Unfortunately, there are not many barium stars with determined binary periods, but there is a trend of decreasing [*s*/Fe] ratio with increasing orbit period—although the scatter seen in this figure would mean that the separation of the stars in the system is not the only parameter that influences the observed overabundances (Jorissen et al. 1998). Dilution effects of the accreted material as well as the metallicity are also important. The star NGC 5822-2 with a period of 1000 days (Mermilliod et al. 1989) displays dynamics and overabundances similar to other field barium stars.

The previous determination of the heavy-element abundance in one of the cluster giant analyzed in this work, NGC 5822-2, was done by Luck (1994), who found [Zr/Fe] = 0.59, which is in good agreement with our results. For the [Nd/Fe] ratio, Luck (1994) found 0.19, which is different from our value of 0.80. This difference of results is probably related to the number of lines employed in the analysis. While our abundance ratio is based on eight lines, the result of [Nd/Fe] of Luck (1994) was based on a single line. Since Luck (1994) used a lower resolution than we used, this single line likely could be contaminated by transitions other than the Nd line.

We may speculate a few reasons why more than 20 yr have passed since the last discovery of a barium star in an open cluster. First, after 2008, when the large radial velocity survey of Mermilliod et al. (2008) was published, several new cluster giants were identified, thus allowing the study of new objects, some of which are binary systems. Second, another important point for the identification of barium stars in an open cluster is the determination of the heavy-element abundances. Few cluster giants have their heavy-element abundances determined; even when they are, the abundances were determined for one or two elements of the *s*-process based on a few lines (Maiorca et al. 2011). Therefore, with new high-resolution spectroscopic surveys to obtain the metallicities and abundances for giants in open clusters, other new barium stars will probably be discovered.

The discovery of these two barium stars in NGC 5822, and the two previously known in NGC 2420, raised another point for a comparison between the frequency of the barium stars to normal giants in field stars and in the cluster. In field stars, the percentage of barium stars is only 1 (MacConnell et al. 1972). In open clusters, the binary frequency of red giant spectroscopic binaries with periods less than 4000 days is 23% (Mermilliod & Mayor 1990). The barium star fraction, considering these two barium stars in NGC 5822 among 21 known giants and two in NGC 2420 among 22, is 10%, 10 times larger than that in the field stars.

5. CONCLUSIONS

Our abundance analysis employing high-resolution optical spectra of two giants in the open cluster NGC 5822 with the aim of obtaining their abundance pattern can be summarized as follows:

1. Stars NGC 5822-2 and NGC 5822-201 are two barium stars found in the open cluster NGC 5822. They have, respectively, a *mean* overabundance of the elements created by slow-neutron capture reactions, "*s*," with the notation [*s*/Fe] of 0.77 ± 0.12 and 0.83 ± 0.05, which is much higher than stars at similar metallicities. HD 65314, a barium star chosen as an *s*-process-enriched comparison star, has [*s*/Fe] = 0.74 ± 0.4. In addition, the luminosities of NGC 5822-2 and -201 are too low for them to be AGB stars and become self-enriched in the elements created by the *s*-process.

   NGC 5822-2 has already been proven as a binary star. Its radial velocity, due to orbital motion, has a systematic variation from -24.5 to -33.5 km s^{-1} (Mermilliod et al. 1989), which is consistent with the mean NGC 5822 radial velocity of -29.31 ± 0.18 (Mermilliod et el. 2008). The previously discovered barium stars in the open cluster NGC 2420, NGC 2420 X and D, have a systematic variation from 81 to 71 km s^{-1} and from 74 to 68 km s^{-1} (Mermilliod et al. 2007), respectively, which is also consistent with the mean NGC 2420 radial velocity of 73.57 ± 0.15 km s^{-1} (Mermilliod et al. 2008). Although NGC 5822-201 displays an enrichment of the elements created by the *s*-process and has already been classified as "SB" (Mermilliod & Mayor 1990), a confirmation of binary status is necessary and very desirable. NGC 5822-201 is probably in a very eccentric orbit where significant radial velocity variations would occur only in a small phase range like in the orbit of star HD 123949, which is seen in Figure 2 of Udry et al. (1998). Another possibility is that the orbit is pole-on.
2. Analysis of the light elements reveals that carbon abundances in NGC 5822-2 and -201 are similar as compared to those in barium stars previously analyzed and also with the barium star HD 65314. Nitrogen abundances show an enrichment similar to field giant stars and other barium stars. The oxygen abundances of NGC 5822-2 and -201 are also similar to those in the field giants as well as to those in other barium stars.
3. Thanks to the radial-velocity survey of Mermilliod et al. (2008), we were able to investigate a "large" sample of

giant stars in the open cluster NGC 5822. NGC 5822 is the second open cluster to host barium stars.

This research used the SIMBAD database, operated at CDS, Strasburg, France.

REFERENCES

Allen, D. M., & Barbuy, B. 2006, A&A, 454, 917
Alonso, A., Arribas, S., & Martínez-Roger, C. 1999, A&AS, 140, 261
Antipova, L. I., Boyarchuk, A. A., Pakhomov, Yu. V., & Panchuk, V. E. 2003, ARep, 47, 648
Antipova, L. I., Boyarchuk, A. A., Pakhomov, Yu. V., & Panchuk, V. E. 2004, ARep, 48, 597
Antipova, L. I., Boyarchuk, A. A., Pakhomov, Yu. V., & Yushkin, M. V. 2005, ARep, 49, 535
Barbuy, B., Jorissen, A., Rossi, S. C. F., & Arnould, M. 1992, A&A, 262, 216
Bessel, M. S., Castelli, F., & Plez, B. 1998, A&A, 333, 231
Bidelman, W. P. 1981, AJ, 86, 553
Blackwell, D. E., Booth, A. J., Menon, S. L. R., & Petford, A. D. 1986, MNRAS, 220, 289
Böhm-Vitense, E., Carpenter, K., Robinson, R., Ake, T., & Brown, J. 2000, ApJ, 533, 969
Boothroyd, A. I., & Sackmann, I. J. 1988, ApJ, 328, 632
Boyarchuk, A. A., Pakhomov, Yu. V., Antipova, L. I., & Boyarchuk, M. E. 2002, ARep, 46, 819
Burbidge, E. M., Burbidge, G. R., Fowler, W. A., & Hoyle, F. 1957, RvMP, 29, 547
Carretta, E., Bragaglia, A., & Gratton, R. G. 2007, A&A, 473, 129
Castro, S., Rich, R. M., Grenon, M., Barbuy, B., & McCarthy, J. K. 1997, AJ, 114, 376
Cayrel, R. 1988, in IAU Symp. 132, The Impact of Very High S/N Spectroscopy on Stellar Physics, ed. G. Cayrel de Strobel & M. Spite (Dordrecht: Kluwer), 345
Chen, Y. Q., Zhao, G., Nissen, P. E., Bai, G. S., & Qiu, H. M. 2003, ApJ, 591, 925
Depagne, E., Hill, V., Spite, M., et al. 2002, A&A, 390, 187
Dobbie, P. D., Day-Jones, A., Williams, K. A., et al. 2012, MNRAS, 423, 2815
Drake, J. J., & Smith, G. 1991, MNRAS, 250, 89
Drake, N. A., & Pereira, C. B. 2011, A&A, 531, 133
Edvardsson, B., Andersen, J., Gustafsson, B., et al. 1993, A&A, 275, 101
Gomez, A. E., Luri, X., Grenier, S., et al. 1997, A&A, 319, 881
Gratton, R. G., & Sneden, C. 1988, A&A, 204, 193
Gray, R. O., McGahee, C. E., Griffin, R. E. M., & Corbally, C. J. 2011, AJ, 141, 160
Grevesse, N., & Sauval, A. J. 1998, SSRv, 85, 161
Hekker, S., & Meléndez, J. 2007, A&A, 475, 1003
Hill, P., Paschmann, G., Treumann, R. A., et al. 1995, JGR, 100, 9575
Hurley, J. R., Pols, O. R., Aarseth, S. J., & Tout, C. A. 2005, MNRAS, 363, 293
Jacobson, H. R., Pilachowski, C. A., & Friel, E. D. 2011, AJ, 142, 59
Jorissen, A., Van Eck, S., Mayor, M., & Udry, S. 1998, A&A, 332, 877
Kaufer, A., Stahl, O., Tubbesing, S., et al. 1999, Msngr, 95, 8
Kovacs, N. 1985, A&A, 150, 232
Kurucz, R. L. 1993, CD-ROM 13, Atlas9 Stellar Atmosphere Programs and 2 km/s Grid (Cambridge, MA: Smithsonian Astrophys. Obs)
Lambert, D. L. 1978, MNRAS, 182, 249
Lambert, D. L. 1981, Physical Processes in Red Giants, Vol. 88 (Dordrecht: Reidel), 115
Lambert, D. L., Heath, J. E., Lemke, M., & Drake, J. 1996, ApJS, 103, 183
Lattanzio, J. C. 1986, ApJ, 311, 708
Lattanzio, J. C., & Wood, P. R. 2004, in Asymptotic Giant Branch Stars, Evolution, Nucleosynthesis and Pulsations of AGB Stars, ed. H. J. Habing & H. Olofsson (Astronomy and Astrophysics Library; Berlin: Springer), 23
Liang, Y. C., Zhao, G., Chen, Y. Q., Qiu, H. M., & Zhang, B. 2003, A&A, 397, 257
Liu, G.-Q., Liang, Y. C., & Deng, L. C. 2009, RAA, 9, 431
Lu, P. 1991, AJ, 101, 2229
Luck, R. E. 1994, ApJS, 91, 309
Luck, R. E., & Heiter, U. 2007, AJ, 133, 2464
MacConnell, D. J., Frye, R. L., & Upgren, A. R. 1972, AJ, 77, 384
Maiorca, E., Randich, S., Busso, M., Magrini, L., & Palmerini, S. 2011, ApJ, 736, 120
Martin, W. C., Fuhr, J. R., Kelleher, D. E., et al. 1999, NIST Atomic Spectra Database Version2.0 (Online Available), NIST Standard Reference Database (Gaithersburg, MD: National Institute of Standards and Technology), http://physics.nist.gov/asd
Masseron, T., Johnson, J. A., Plez, B., et al. 2010, A&A, 609, 93
McClure, R. D., Forrester, W. T., & Gibson, J. 1974, ApJ, 189, 409
McWilliam, A., & Rich, M. R. 1994, ApJS, 91, 749
Mennesier, M. O., Luri, X., Figueras, F., et al. 1997, A&A, 326, 722
Mermilliod, J. C., Andersen, J., Latham, D. W., & Mayor, M. 2007, A&A, 473, 829
Mermilliod, J. C., & Mayor, M. 1990, A&A, 237, 61
Mermilliod, J. C., Mayor, M., Andersen, J., et al. 1989, A&AS, 79, 11
Mermilliod, J. C., Mayor, M., & Udry, S. 2008, A&A, 485, 303
Mishenina, T. V., Bienaymé, O., Gorbaneva, T. I., et al. 2006, A&A, 456, 1109
Pace, G., Danziger, J., Carraro, G., et al. 2010, A&A, 515, 28
Pereira, C. B., & Drake, N. A. 2009, A&A, 496, 791
Pereira, C. B., & Drake, N. A. 2011, AJ, 141, 79
Pereira, C. B., Sales Silva, J. V., Chavero, C., Roig, F., & Jilinkski, E. 2011, A&A, 533, 51
Reddy, B. E., Bakker, E. J., & Hrivnak, B. J. 1999, ApJ, 524, 831
Reddy, B. E., Tomkin, J., Lambert, D. L., & Allende Prieto, C. 2003, MNRAS, 340, 304
Reyniers, M., Van Winckel, H., Gallino, R., & Straniero, O. 2004, A&A, 417, 269
Santos, N. C., Lovis, C., Pace, G., Melendez, J., & Naef, D. 2009, A&A, 493, 309
Smiljanic, R., Gauderon, R., North, P., et al. 2009, A&A, 502, 267
Smiljanic, R., Porto de Mello, G. F., & da Silva, L. 2007, A&A, 468, 679
Smith, V. V. 1984, A&A, 132, 326
Smith, G., Edvardsson, B., & Frisk, U. 1986, A&A, 165, 126
Smith, V. V., Cunha, K., Jorissen, A., & Boffin, H. M. J. 1996, A&A, 315, 179
Smith, V. V., & Suntzeff, N. B. 1987, AJ, 93, 359
Sneden, C. 1973, PhD thesis, Univ. Texas
Sneden, C., McWilliam, A., Preston, G. W., et al. 1996, ApJ, 467, 819
Twarog, B. A., Anthony-Twarog, B. J., & McClure, R. D. 1993, PASP, 105, 78
Udry, S., Jorissen, A., Mayor, M., & Van Eck, S. 1998, A&AS, 131, 25
Van Winckel, H., & Reyniers, M. 2000, A&A, 345, 135
Vassiliadis, E., & Wood, P. R. 1993, ApJ, 413, 641
Von Hippel, T., Gilmore, G., & Jones, D. H. P. 1995, MNRAS, 273, L39
Wiese, W. L., Smith, M. W., & Miles, B. M. 1969, NSDRS-NBS, 68
Začs, L. 1994, A&A, 283, 937